RESEARCH ARTICLE



MEDICAL PHYSICS

Longitudinal in silico imaging study comparing digital mammography and digital breast tomosynthesis systems

Miguel A. Lago | Aldo Badano

U.S. Food and Drug Administration, Silver Spring, Maryland, USA

Correspondence

Miguel A. Lago, U.S. Food and Drug Administration, Silver Spring, MD 20993, USA. Email: miguel.lago@fda.hhs.gov

Abstract

Background: In silico clinical trials are becoming more sophisticated and allow for realistic assessment and comparisons of medical image system models. These fully computational models enable fast and affordable trial designs that can closely capture trends seen on real clinical trials.

Purpose: To evaluate three breast imaging system models for digital mammography (DM) and digital breast tomosynthesis (DBT) in a fully-in-silico longitudinal study.

Methods: We developed in silico models for three different breast imaging systems by modeling relevant characteristics such as detector technology, pixel size, number of projections, and angular span. We use a computational image reader to detect masses at different growing stages to compute the relative system performance. Similarly, we compare calcification cluster detectability across systems. The Detectability area under the ROC curve (AUC) was calculated for each combination of breast density, device model, lesion size and type, and search area. We compared the absolute and relative AUC values for DM and DBT. The trial consisted of 45 000 simulated images corresponding to 750 virtual digital patient models.

Results: We observed proportional AUC values with increasing mass size. On the other hand, higher breast densities showed lower AUC values. For masses, we found significant performance differences between device models. The highest average AUC difference between DBT and DM was 0.109, benefiting DBT. For calcifications, DM showed higher performance than DBT, especially in highly dense breasts. The highest AUC difference on a model was -0.055, benefiting DM.

Conclusions: In this fully-in-silico imaging trial, we compared three imaging systems with different detector technologies on the same cohort of virtual digital patient models. We found that breast device systems can lead to visibility differences in masses and calcifications. Our longitudinal, multi-device in silico study was possible because of the versatility and flexibility of in silico methods. This study shows the advantages of this in silico methodology in lowering the resources needed for device development, optimization, and regulatory evaluation.

KEYWORDS

breast imaging, in silico, virtual clinical trials

Published 2024. This article is a U.S. Government work and is in the public domain in the USA.

1 | INTRODUCTION

The Food and Drug Administration (FDA) has, at this writing, approved five different devices for x-ray-based screening breast imaging from four companies. 1, 2 Although using the same fundamentals, they have differences in their underlying technology including in such areas as detector technology, number of projections, and reconstruction algorithms. However, the influences of such technological differences on cancer detectability are currently unclear. Typically, characterization of x-ray imaging devices is performed by measuring their noise power spectrum (NPS) and modulation transfer function (MTF).3 Although these two metrics can provide information about the amount of noise on, and general sharpness of, the produced images, they might not be relevant for clinical tasks that involve nonlinear 3D image reconstruction. Understanding how detectability of clinically relevant lesions (e.g., calcification clusters, masses) for a range of devices helps discern the impact of the devices' technological differences on patients.

An emerging field for testing and comparing medical devices is in silico imaging trials.^{4–6} In silico trials are partially or completely composed of computational simulations and models of the objects, imaging devices and processes of interest. They enable faster development of clinical devices and accelerates the validation of existing ones.^{7–9} Badano et al.¹⁰ reported a full in silico imaging trial for breast cancer detection that replicated the results of a real-world clinical trial.

In this paper, we discuss an expanded in silico trial pipeline Virtual Imaging Clinical Trial for Regulatory Evidence (VICTRE)^{11, 12} to study the performance of three breast imaging systems models (ISM) for the detection of growing breast masses and calcification clusters over time. These models are based on some of the characteristics for FDA-approved commercial systems, including the GE Healthcare SenoClaire (ISM A), the Hologic Inc. Selenia Dimensions (ISM B), and the Siemens Inspiration (ISM C). Using an anatomy-informed growing mass simulation model,^{12–14} and the detector models presented by Sengupta et al.,³ we analyzed the performance for detecting mass lesions at different growing stages and calcification clusters in three breast imaging systems.

2 | MATERIALS AND METHODS

2.1 | Trial population

We generated 750 different breast models on four breast densities (extremely dense, heterogenously dense, scattered density, and fatty) in which we inserted either a growing mass at one of five sizes or a calcifica-

tion cluster. The total number of digital mammography (DM) and digital breast tomosynthesis (DBT) simulations were $750 \times (4 \text{ masses} + 1 \text{ cluster}) \times (3 \text{ devices}) \times (4 \text{ breast densities}) = 45\,000$ (Figure 1). All cases were simulated on the FDA Center for Devices and Radiological Health's High Performance Computing (HPC) Cluster using parallel executions of each ISM.

2.2 | Breast model

The in silico model of the breast was generated using Graff's open-source model. This anthropomorphic model can generate stochastic knowledge-based breast models with a complex array of internal tissues including adipose tissue, glandular compartments, veins, arteries, Cooper's ligaments, and others. The model also includes a list of candidate lesion locations determined by the position of the terminal duct lobular units, which we used later when inserting lesions.

Breast density was modeled after the four categories studied in the original VICTRE trial. These categories correspond to four dense-to-glandular tissue, ratios where size is inversely proportional to breast density. Densities are constant and any internal tissue is static during the lesion-growing process. Further optimizations of the breast model could include a breast density reduction over time and tissue displacement coupled with the lesion-growing algorithm.

To simulate the compression paddle on a breast imaging device, the model is converted into a finite element model by transforming the voxelized volume to a tetrahedral mesh. The corresponding tetrahedral model is placed between two rigid plates that simulate the tissue compression using the open-source software FEBio.¹⁷ Finally, the compressed tetrahedral model is converted back to a voxelized volume.

The lesion growth model was developed by Sengupta et al. 12–14 and simulates the internal growth of a breast mass tumor. Growth of these mass models is driven by the interstitial tumor pressure, concentration of metabolites, and stiffness of the local tissues. The growing location of the tumor is randomly selected from the list of candidate locations based on the model generation. Cell pressure and growth is calculated based on surrounding material composition, nutrients, and cell phenotypes. Active cells with enough energy to divide proliferate and grow the tumor in a chosen direction around them. Selected growing directions are based on the pressure from neighboring cells. The probability of growth is inversely proportional to the stiffness of the surrounding tissue (i.e., the tumor will grow less towards

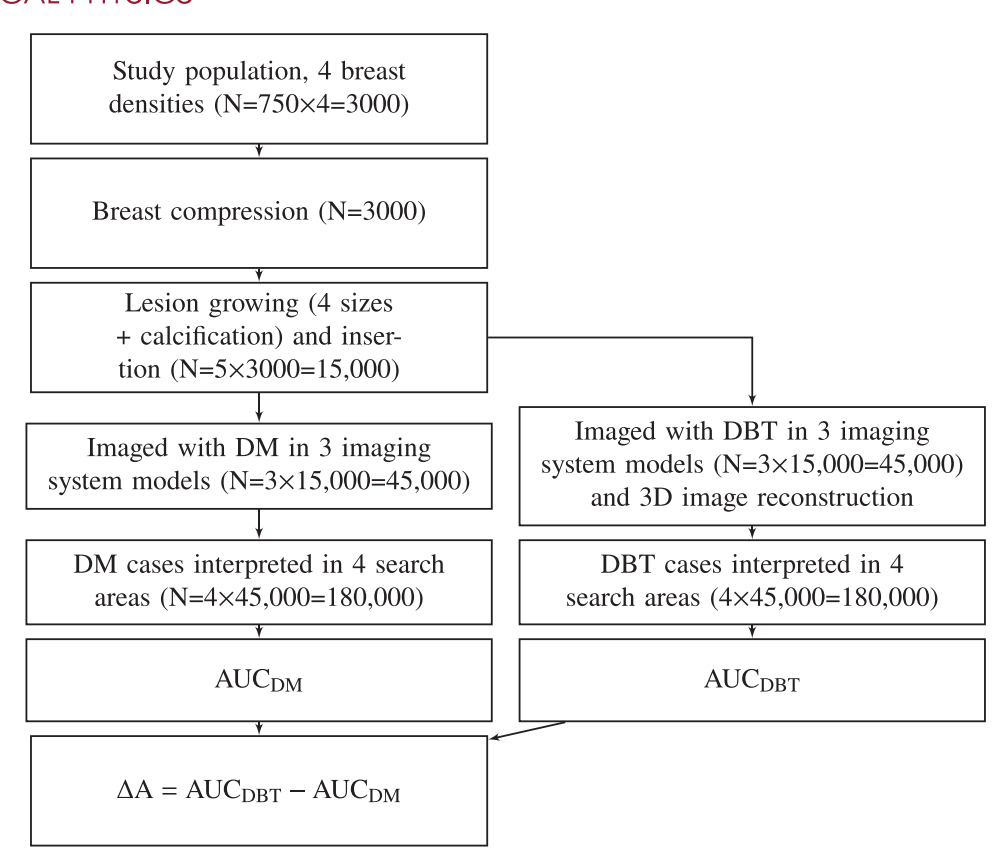


FIGURE 1 Flowchart of the virtual patient population and study analysis.



FIGURE 2 Central slice for a growing lesion model at eight consecutive timepoints.

more rigid materials such as glandular tissue or ligaments). Initial location of the tumor growth therefore defines its final shape and size, resulting in each mass having a unique morphology. Data on tumor size were extracted at different growing points and ranged from an average radius of $\sim\!\!1$ mm for the smallest lesion size to $\sim\!\!3.5$ mm for the largest lesion size (see Figure 2 for an example of a growing mass). The growing rate was identical in all cases.

Additionally, we designed random calcification clusters from 8 to 20 calcifications and sizes of 0.05 to 0.15 mm in a maximum volume of 5 mm per side. These clusters differ on each realization and were randomized based on parameters controlling size, number of calcifications, and cluster maximum volume span. Clusters are generated as a single instance and are not studied over time, therefore, only one time point was reported.

2.4 | Imaging system model

We simulated the geometry of three different breast ISM using Monte Carlo simulations with MCGPU.^{19,20} Table 1 shows the variability added to these ISMs in terms of detector pixel size, number of DBT projections, and detector model used as in Sengupta et al.3 These ISMs were used to produce one planar DM image and a volumetric DBT image of each of the exact same breast models for a direct comparison. The simulated ISMs do not fully represent the commercial devices since some parameters were not part of this study. For instance, the pixel pitch of the ISM B for the DBT is binned on a 2×2 square and the reconstruction software are proprietary algorithms. All other parameters for the ISMs not mentioned here were taken from the original VICTRE trial 10, 21, 22 (See Supplementary Material).

TABLE 1 Device characteristics modeled in MCGPU as input parameters for the simulation of different devices.

	ISM A	ISM B	ISM C
Pixel pitch (μm)	100	70	85
Detector technology	Csl	a-Se	a-Se
Detector thickness	0.025 mm Rh	0.02 mm Rh	0.02 mm Rh
# DBT projections	9	15	25
DBT angle range	±12.5°	±7.5°	±25°
Reconstruction	FBP	FBP	FBP

Note: Detector technologies are simulated following Sengupta et al.³ Abbreviations: Csl, cesium lodine; a-Se. amorphous selenium; DBT, digital breast tomosynthesis; FPB, filtered back projection; ISM, imaging systems model; Rh, rhodium.

2.5 | Image interpretation model

Typically, channelized Hotelling observers (CHOs) have been used to assess the detectability of lesions on breast images.^{23, 24} A reader model (or model observer) integrates a template based on the average signal (i.e., breast lesion) and the average background statistics (i.e., breast parenchyma). To calculate the average lesion, we took the average gray level for all lesions centered in the same pixel, this is necessary since lesions grow differently on each case thus making it impossible to do a signal-known template. Average background statistics are calculated in a similar way, averaging multiple realizations of the background without a signal and using the covariates. We chose a CHO using Laguerre–Gauss channels with parameters adjusted to the size of the signal²⁵ (see Supplementary Material).

The reader model template was generated by optimally combining the five channels into a single linear template.

$$\mathbf{v} = \mathbf{T}^t \mathbf{g} \tag{1}$$

$$\mathbf{K}_{\mathbf{v}} = \text{cov}(\mathbf{v})$$
 (2)

where T is the channels matrix and g is the set of training trials. Finally, we calculated the channel covariance matrix K_v and, along with the average signal s, we integrate the CHO template:

$$\mathbf{w}_{\text{CHO}} = \mathbf{T}\mathbf{K_v}^{-1}\mathbf{T}^t\mathbf{s} \tag{3}$$

In previous works, image readers consider the location of the signal perfectly known and only test one location. However, this is not realistic since radiologists are usually not aware of the potential locations, of the lesions and need to search in large areas of the image. Therefore, in addition to the location-known-exactly (LKE) paradigm, the reader models in our study performed a small search around each signal's potential location. Typically, larger search areas increase the likelihood of evaluating false positive locations constitutions.

plicating the detection task. On the other hand, while a mass can be localized by its centroid, a calcification cluster does not have one unique center and the search area depends on the distribution of the several single calcifications. Thus, we studied the performance of our reader models on different search area sizes for both masses and calcification clusters. The largest search area was defined as a square region of interest (ROI) of 59×59 px for the DM and $59 \times 59 \times 7$ vx for the DBT whereas the smallest was one single pixel or voxel. For search areas, the template ${\bf w}$ was convolved with the search area was taken as the response for that trial.

Note that, since calcification clusters are different on each realization, no true template includes all the calcifications. We decided to use a single-calcification template to search for all calcifications present in the search area. An LKE strategy is not optimal in this case for two main reasons: (1) the clusters are not centered on a single pixel, and (2) the clusters are randomized with different number and size of calcifications on each instance. We opted to have a minimum search area for these clusters so we avoid reducing it so much so that they are never seen as could happen for LKE (1 pixel only). Therefore, calcification clusters are always considered only for a search task.

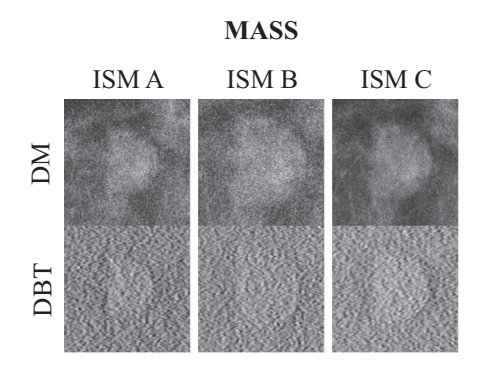
3 | RESULTS

Figure 3 shows the same mass and calcification cluster as seen by the three different ISMs on both DM and DBT (central slice) modalities. Signal sizes appear different because we extracted the same ROI of 159×159 px on devices with different pixel size. Due to ISM B having a smaller pixel size, signals appear larger. Also, since DBT technology has multiple slices and ISMs have diverse number of slices, slice thickness, and angle ranges; calcification clusters are harder to see on a single slice.

We computed the corresponding dose received by the glandular tissue on each of the ISMs. Figure 4 shows a histogram of each of the four densities on the three different ISMs. Comparisons show high agreement on the dose levels each of the models received, indicating that the imaging was performed at a similar level of radiation dose. These dose distributions follow trends reported in previous research.^{10, 20}

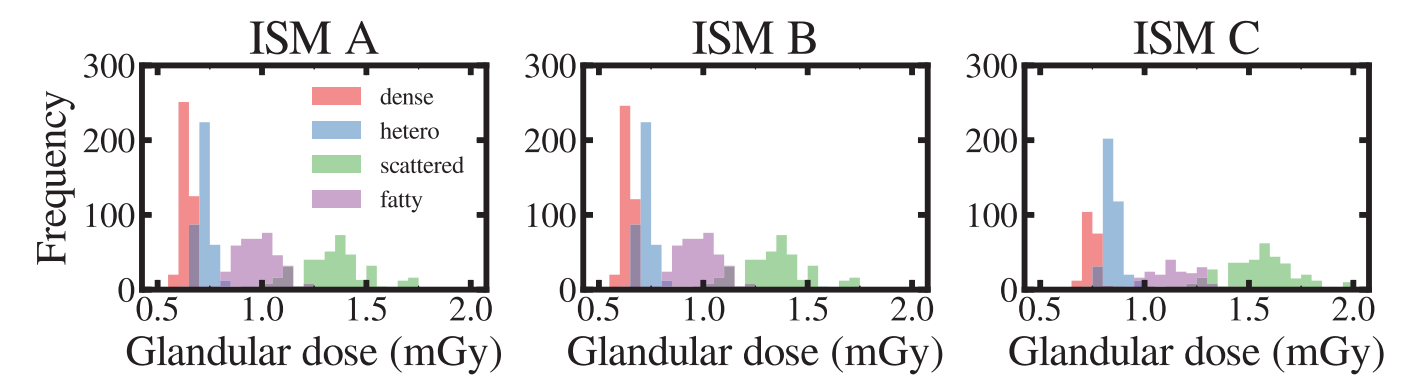
Figure 5 compares reader model performance for each mass size on LKE and increasing search areas. The area under the ROC curve (AUC) values follow an increasing trend proportional to the lesion radius. In terms of density, results also show a proportional increase in AUC with lower density cases.

Figure 6 shows the relative difference between DBT and DM for each mass size, search area, as well as for calcification clusters. For masses, in most cases, DBT outperformed DM modality as seen in previous studies.



CALCIFICATION CLUSTER ISM B ISM C ISM A DM DBT

Sample ROIs (159 x 159 px) for the three ISMs for a mass at 2.5 mm radius and a calcification cluster with 16 calcifications. DBT is the central slice of the signal center. Note that pixel size is different on each ISM; therefore signals appear with different sizes for the same ROI. Images are contrast enhanced for visualization purposes. DBT, digital breast tomosynthesis; ISMs, imaging systems models; ROI, region of interest.



Dose distribution for each breast density on each device model for DM modality. Similar doses were used for DBT across the number of projections. DBT, digital breast tomosynthesis; DM, digital mammography.

In cases with larger search areas, DM shows better AUC than DBT (especially for higher-density breasts), which may result from the lower performance of model observers on larger search areas.

Table 2 shows the weighted averages for all densities together considering the following proportions: dense (10%), heterogenously dense (40%), scattered density (40%), and fatty (10%). Results for all mass sizes are taken from the LKE data; for calcifications results are taken from the largest search area data. ΔAUC is also calculated as the difference AUC_{DRT} – AUC_{DM}.

4 DISCUSSION

For masses, we see a monotonic increase in AUC values proportional to the lesion radius (Figure 5). ISM A outperformed the other two ISMs on DM for larger lesion sizes. ISM B seems to be less sensitive to mass size and lower AUC. This model also shows a reversal in AUC trend in larger masses and some breast densities. This could be a sign of an underperforming reader model on larger masses (e.g., channel choice is not optimal),

Weighted AUC averages for each mass size (LKE) and calcifications (largest search area) for each ISM on DM and DBT.

	` •	,		
	Lesion size (mm)	AUC_{DM}	AUC _{DBT}	ΔAUC
ISM A	0.86	0.716	0.806	0.090
	1.63	0.813	0.847	0.034
	2.43	0.806	0.857	0.051
	3.51	0.838	0.868	0.030
	CALC	0.580	0.525	-0.055
ISM B	0.86	0.712	0.782	0.069
	1.63	0.765	0.852	0.087
	2.43	0.770	0.871	0.101
	3.51	0.727	0.864	0.137
	CALC	0.579	0.546	-0.033
ISM C	0.86	0.714	0.823	0.109
	1.63	0.777	0.873	0.096
	2.43	0.797	0.896	0.099
	3.51	0.823	0.907	0.084
	CALC	0.593	0.550	-0.043

Abbreviations: AUC, area under the ROC curve; DBT, digital breast tomosynthesis; DM, digital mammography; ISM, imaging systems model; LKE, locationknown-exactly.

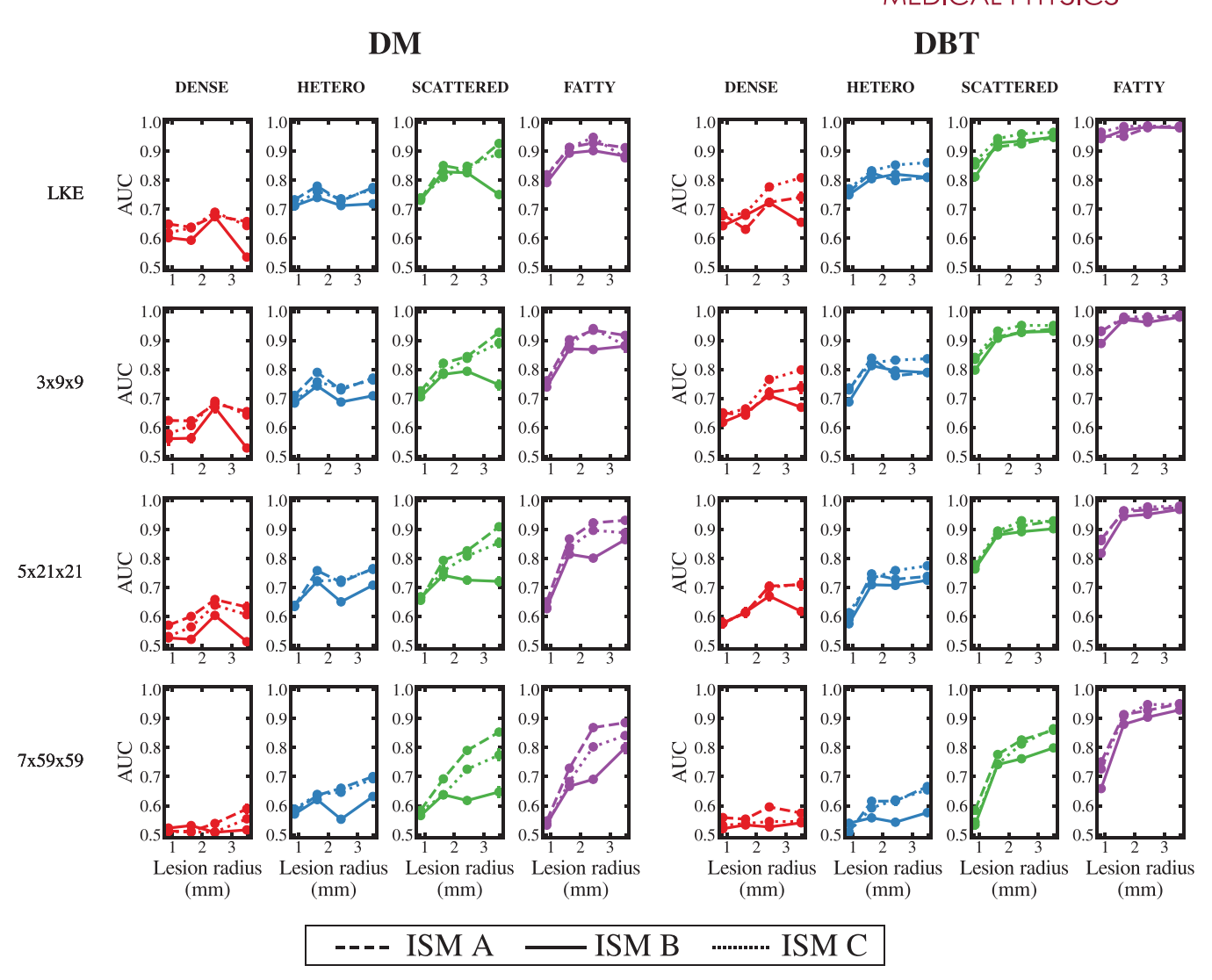


FIGURE 5 AUC results for the different mass sizes for DM and DBT for each of the search areas on three different ISMs. AUC, area under the ROC curve; DBT, digital breast tomosynthesis; DM, digital mammography; ISMs, imaging systems models.

or background features being closer to some specific mass sizes.

As breast density decreases, all ISMs showed higher AUCs, indicating that, when masses are located on dense breasts, they are most affected by tissue occlusion. Finally, in almost all cases, and especially on lower densities, masses were more visible on DBT than DM. This finding agrees with previous in silico¹⁰ and clinical trial results.

On the other hand, calcification clusters seem to be more detectable in dense breasts than in fatty breasts on DM images, possibly due to the size differences that cause more overlapping tissues to confound the reader models for this type of signal. In all but fatty densities, DM outperformed DBT, with varying degrees of significance. ISMs differences benefit DM versus DBT, with some cases showing higher significance, especially ISM C on dense and heterogenously dense and ISM

B on scattered density. We will continue to investigate this result.

In terms of search areas, larger search areas have lower overall AUC values on both DM and DBT for all models and lesion sizes. Search areas serve in two different ways: (1) the fact that the reader model is not only looking at a single location, which introduces more variability and increases the difficulty of the task, and (2) although we did not use large search areas, radiologists always start locating suspicious ROIs and later characterizing them as malignant or benign. Adding a small search on these regions accounts for exploring the surroundings and not only a single pixel (voxel) location for the determination of absence or presence of the signal.

Computing the detectability of calcification clusters with traditional model observers presents some challenges. First, since we randomized their size, number, and position, each realization had a different

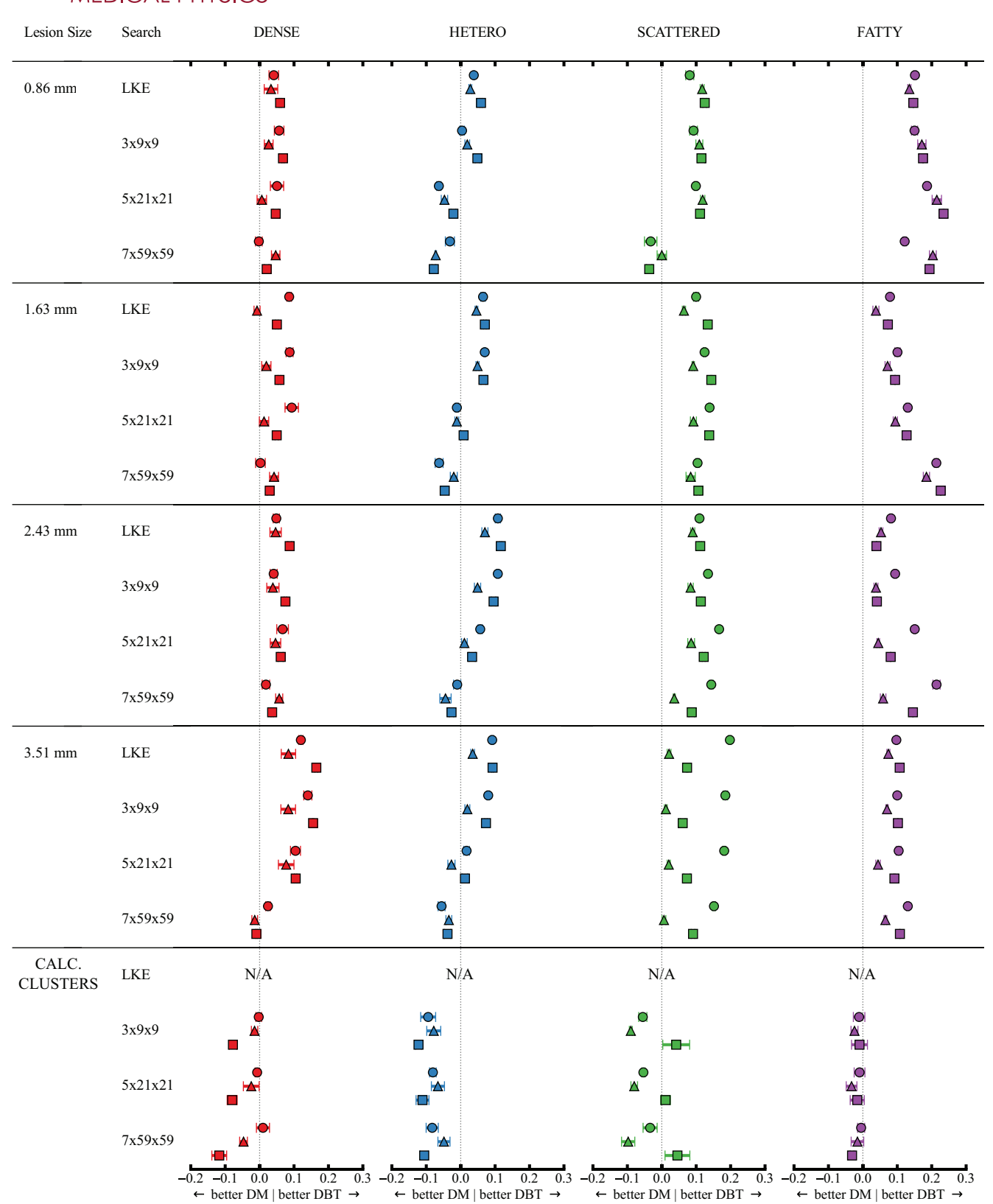


FIGURE 6 Relative AUC reader model performance for the detection of masses at different sizes and calcification clusters on three different ISMs between DM and DBT modalities. Error bars are 95% confidence intervals. AUC, area under the ROC curve; CALC, calcifications; DBT, digital breast tomosynthesis; DM, digital mammography; ISMs, imaging systems models; LKE, location-known-Exactly.

organization and difficulty. Although this randomization increased the realism of images we generated, it decreased the efficiency of our reader models. Comparing the different ISMs on calcifications, we see that benefits from DM is more apparent on denser breasts and with ISMs B and C. Comparing smaller search areas for calcifications is almost irrelevant since a cluster spans more than the search area, which means some calcifications are outside it and therefore are never seen by the reader model. Density seems to affect the relative AUC, with denser breasts benefiting from DM and fattier breasts benefiting from DBT. We note that the CHO models do not consider the pixel size for each model, and that might cause small performance variability. However, the model training is performed especially for each ISM, hence including pixel size in this process.

5 | CONCLUSIONS

We present the results of the first fully detailed longitudinal in silico study comparing the detectability of realistic growing masses and random calcification clusters using three different breast imaging system models.

The study presented here highlights the benefits of in silico clinical trials. A study this size, in real life, would have prohibitive costs both in time and money, in addition to the ethical concerns around monitoring a cohort of patients with known growing tumors for months or years.

The results from this experiment reflect trends seen in real clinical study results and provide encouragement for using in silico clinical trials as part of medical image development and regulatory evaluation.

ACKNOWLEDGMENTS

Vanday Bundu (FDA), contributed on the code portion for the lesion growing algorithm. The authors thank Joanne Berger, FDA Library, for manuscript editing assistance. We express gratitude to the members of the VICTRE team for their feedback on the trial design and methods.

CONFLICT OF INTEREST STATEMENT

The mention of commercial products, their resources, or their use in connection with material reported herein is not to be construed as either an actual or implied endorsement of such products by the Department of Health and Human Services. This is a contribution of the U.S. Food and Drug Administration and not subject to copyright.

REFERENCES

 Mackenzie A, Marshall NW, Hadjipanteli A, Dance DR, Bosmans H, Young KC. Characterisation of noise and sharpness of images from four digital breast tomosynthesis systems for simulation of images for virtual clinical trials. *Phys Med Biol.* 2017;62(6):2376-2397. doi:10.1088/1361-6560/aa5dd9

- Ikejimba LC, Salad J, Graff CG, et al. Assessment of task-based performance from five clinical DBT systems using an anthropomorphic breast phantom. *Med Phys.* 2021;48(3):1026-1038. https://aapm.onlinelibrary.wiley.com/doi/abs/10.1002/mp.14568
- Sengupta A, Badal A, Makeev A, Badano A. Computational models of direct and indirect x-ray breast imaging detectors for in silico trials. *Med Phys.* 2022;49(11):6856-6870. https://aapm.onlinelibrary.wiley.com/doi/abs/10.1002/mp.15935
- Abadi E, Segars WP, Tsui BM, et al. Virtual clinical trials in medical imaging: a review. *J Med Imaging Radiat Oncol*. 2020;7(4):042 805-042 805. doi:10.1117/1.JMI.7.4.042805
- Badano A, Lago, MA, Sizikova, E, et al. The stochastic digital human is now enrolling for in silico imaging trialsmethods and tools for generating digital cohorts. *Prog biomed eng.* 2023;5(4):042002. doi:10.1088/2516-1091/ad04c0
- Badano A. In silico imaging clinical trials: cheaper, faster, better, safer, more scalable. *Trials*. 2021;22(1):1-7. doi:10.1186/s13063-020-05002-w
- Abadi E, Barufaldi B, Lago M, et al. Toward widespread use of virtual trials in medical imaging innovation and regulatory science. Med Phys. 2024. doi:10.1002/mp.17442
- Vancoillie L, Marshall N, Cockmartin L, Vignero J, Zhang G, Bosmans H. Verification of the accuracy of a hybrid breast imaging simulation framework for virtual clinical trial applications. *J Med Imaging Radiat Oncol*. 2020;7(4):042 804-042 804. doi:10. 1117/1.JMI.7.4.042804
- Barufaldi B, Higginbotham D, Bakic PR, Maidment AD. OpenVCT: a GPU-accelerated virtual clinical trial pipeline for mammography and digital breast tomosynthesis. In: *Medical Imaging 2018: Physics of Medical Imaging*. Vol 10573. SPIE; 2018:1333-1340. doi:10.1117/12.2294935
- Badano A, Graff CG, Badal A, et al. Evaluation of digital breast tomosynthesis as replacement of full-field digital mammography using an in silico imaging trial. *JAMA Netw Open*. 2018;1(7): e185474. https://jamanetwork.com/journals/jamanetworkopen/ article-abstract/2717000
- VICTRE: In silico breast imaging pipeline (RST24MD10.01).
 2023. https://github.com/DIDSR/VICTRE_PIPELINE/
- Lago MA, Sengupta A, Badano A. Design of an in silico imaging trial with growing breast cancer lesions: comparison between DM and DBT detectability. In: *Medical Imaging 2023: Physics of Medical Imaging*. Vol 12463. SPIE; 2023:253-258. doi:10.1117/12.2653278
- Sengupta A, Sharma D, Badano A. Computational model of tumor growth for in silico trials. In: Medical Imaging 2021: Physics of Medical Imaging. Vol 11595. SPIE; 2021:1262-1270. doi:10.1117/ 12.2580787
- Sengupta A, Lago M, Badano A. In situ tumor model for longitudinal in silico imaging trials. *Phys Med Biol.* 2024;69(7):075029. http://iopscience.iop.org/article/10.1088/1361-6560/ad3322
- Graff CG. A new, open-source, multi-modality digital breast phantom. In: Kontos D, Flohr TG, eds. Medical Imaging 2016: Physics of Medical Imaging. International Society for Optics and Photonics Vol 9783. SPIE; 2016:978309. doi:10.1117/12.2216312
- Checka CM, Chun JE, Schnabel FR, Lee J, Toth H. The relationship of mammographic density and age: implications for breast cancer screening. Am J Roentgenol. 2012;198(3):W292-W295. doi:10.2214/AJR.10.6049
- Maas SA, Ellis BJ, Ateshian GA, Weiss JA. FEBio: finite elements for biomechanics. J Biomech Eng. 2012;134(1):011005. doi:10.1115/1.4005694
- Egan R, McSweeney M, Sewell C. Intramammary calcifications without an associated mass in benign and malignant diseases. *Radiology*. 1980;137(1):1-7. doi:10.1148/radiology.137. 1.7422830
- Badal A, Badano A. Fast simulation of radiographic images using a Monte Carlo x-ray transport algorithm implemented in CUDA. In:

24734209, 2025, 3, Downloaded from https://aapm.onlinelibrary.wiley.com/doi/10.1002/mp.17571 by University Of Nevada Reno, Wiley Online Library on [12/10/2025]. See the Terms inditions) on Wiley Online Library for rules of use; OA articles are governed by the applicable Creative Commons

- GPU Computing Gems Emerald Edition. Elsevier; 2011:813-829. doi:10.1016/B978-0-12-384988-5.00050-4
- Badal A, Sharma D, Graff CG, Zeng R, Badano A. Mammography and breast tomosynthesis simulator for virtual clinical trials. Comput Phys Commun. 2021;261:107779. https://www.sciencedirect. com/science/article/pii/S0010465520303891
- Sengupta A, Zeng R, Sharma D, Badano A. The first freely available open source software package for performing 3D image reconstruction for digital breast tomosynthesis. In: Lo JY, Schmidt TG, Chen G-H, eds. *Medical Imaging 2018: Physics of Medical Imaging.* Vol 10573. International Society for Optics and Photonics. SPIE; 2018:1435-1440. doi:10.1117/12. 2293146
- Sharma D, Graff CG, Badal A, et al. In silico imaging tools from the VICTRE clinical trial. *Med Phys*. 2019;46(9):3924-3928. https://aapm.onlinelibrary.wiley.com/doi/abs/10.1002/mp.13674
- Barrett HH. Objective assessment of image quality: effects of quantum noise and object variability. JOSA A. 1990;7(7):1266-1278. doi:10.1364/JOSAA.7.001266
- Burgess A. Image quality, the ideal observer, human performance of radiologic decision tasks. *Acad Radiol.* 1995;2(6):522-526. doi:10.1016/s1076-6332(05)80411-8
- Park S, Barrett HH, Clarkson E, Kupinski MA, Myers KJ. Channelized-ideal observer using Laguerre-Gauss channels in detection tasks involving non-Gaussian distributed lumpy back-

- grounds and a gaussian signal. *JOSA A*. 2007;24(12):B136-B150. doi:10.1364/JOSAA.24.00B136
- He X, Samuelson F, Zeng R, Sahiner B. Discovering intrinsic properties of human observers' visual search and mathematical observers' scanning. J Opt Soc Am A. 2014;31(11):2495-2510. https://www.osapublishing.org/abstract.cfm?uri=josaa-31-11-2495
- Lago MA, Jonnalagadda A, Abbey CK, et al. Under-exploration of three-dimensional images leads to search errors for small salient targets. *Curr Biol.* 2021;31(5):1099-1106. http://www. sciencedirect.com/science/article/pii/S0960982220318819
- Popescu LM, Myers KJ. CT image assessment by low contrast signal detectability evaluation with unknown signal location. *Med Phys.* 2013;40(11):111908. https://aapm.onlinelibrary.wiley.com/ doi/abs/10.1118/1.4824055

How to cite this article: Lago MA, Badano A. Longitudinal in silico imaging study comparing digital mammography and digital breast tomosynthesis systems. *Med Phys*. 2025;52:1960–1968.

https://doi.org/10.1002/mp.17571